Near-field noise measurements of a high-performance military jet aircraft[1)2)3)]

Alan T. Wall[a)], Kent L. Gee[b)], Michael M. James[c)], Kevin A. Bradley[c)], Sally A. McInerny[c)] and Tracianne B. Neilsen[b)]

**Published near-field analyses of full-scale jet noise are limited, and the application of observed laboratory-scale phenomena to full-scale jets is not well understood. To obtain a greater understanding of the connection between radiated noise and source characteristics in full-scale, heated, supersonic jets produced by military aircraft, extensive acoustical measurements were made in the geometric near field of the jet produced by the installed engine on an F-22A Raptor. In this paper, the experimental setup is described in detail. Level-based results are shown, including overall levels, spectral content and how the spectra vary over space. In addition, basic time waveform analyses are performed. From these results, important near-field jet-noise phenomena are identified, and several technical and logistical issues in implementing near-field measurements of full-scale jets are addressed. © *2012 Institute of Noise Control Engineering.*

Primary subject classification: 13.1.5; Secondary subject classification: 74.7

---

1 INTRODUCTION

The noise radiated from jets on military aircraft is not well understood because characteristics unique to supersonic, high-temperature, full-scale engines have not previously been widely investigated. A connection must be established between turbulent flow structures in a jet and radiated noise in order to understand and improve the impact of noise control measures. Extensive measurements were made in the geometric near field of a high-performance military aircraft to characterize the acoustic environment of maintainer personnel, and to provide greater understanding of full-scale jet noise phenomena[1–3]. The purpose of this paper is threefold: First, this paper describes the experiment in depth, so it serves as a reference for future work. Second, it provides basic analyses of near-field properties and source characteristics that are inferred from these properties, with a focus on phenomena unique to full-scale jet engine noise. Finally, this paper offers insights into sound field characteristics that are useful for the practical implementation of high-power jet noise experiments.

The majority of today's jet noise studies have been limited to smaller, laboratory-scale tests. Some acoustical data are available for high Mach number flows[4–7], but test facilities are generally scale, temperature and velocity-limited. Several notable studies have been performed of model-scale jets in the near field[8–10] and others of full-scale jets in the far field[11–13], but studies performed in the near field of military-type jets are few[14]. This study reports the experimental procedures

of, and addresses some jet-noise phenomena observed from measurements made in the geometric near field of the jet produced by an installed engine on an F-22A Raptor.

Section 2 of this paper describes the experiment, including details about the aircraft and test environment, the design of the array-based measurements, the data acquisition system and the test procedures. Section 3 provides results of measured jet-noise quantities, such as overall sound pressure levels (OASPLs), the spatial variation of spectral content and basic time-waveform properties. From these results characteristics about the maintainer environment are provided, frequency-dependent radiation patterns are observed, two separate spectral peaks unique to full-scale jets are identified and nonlinear acoustic shock content is shown. Throughout the paper, issues concerning technical and logistical challenges encountered in performing full-scale jet-noise experiments are addressed.

2 EXPERIMENT OVERVIEW

More than 6000 measurement points and the repetition of the measurement over four engine conditions make this the most extensive near-field measurement of a jet on a high-performance military aircraft to date. The experiment was primarily designed for a near-field acoustical holography analysis[3,15–18] although holography results are not presented in this paper. This section summarizes the measurements made. First, details about the aircraft, test environment, microphone arrays and data acquisition system are presented. Then the test sequence is outlined. Additional details about the experiment are described elsewhere by James et al[1] and by James and Gee[2].

2.1 Aircraft

Researchers at Blue Ridge Research and Consulting and Brigham Young University conducted static run-up tests on the Lockheed Martin/Boeing F-22A Raptor (shown in Fig. 1) during 27–30 July 2009 at Holloman Air Force Base (HAFB), New Mexico. The F-22A Raptor has two Pratt & Whitney F119-PW-100 turbofan engines that are each in the 160 kN (35,000 lbf) thrust class. The engines have two-dimensional convergent-divergent nozzles capable of $\pm 20°$ thrust vectoring. The engine closest to the measurement arrays was cycled through four power conditions: idle, intermediate, military, and full afterburner, while the other engine was held at idle.

For the purposes of this experiment, the focus is on radiation into the environment of the aircraft maintainer, to the side of the jet. Since all measurements were taken in this region, the noise variation with the

change in azimuthal direction is unknown. (For studies on the effects of non-axisymmetric nozzle geometries, the reader is directed to Refs. 19 and 20.) The nozzle exit of each engine is centered 1.91 m above the ground and has a rectangular aspect ratio of approximately 1:2, although the variable thrust-vectoring components cause the nozzle shape to change with different engine conditions.

2.2 Test Environment

During the static run-up measurements, the aircraft was tied down in the center of a 24.4 m (80 ft) wide concrete ground run-up pad. Rain-packed dirt was on either side of the pad, making the terrain very flat. A blast deflector was located approximately 30 m (100 ft) directly behind the aircraft. On the measurement side of the run-up pad, there was also a small building approximately 25 m to the side and slightly forward of the nozzle exit, and a short wall running almost parallel to and 30 m from the jet centerline. These obstructions precluded measurement locations in the far field. Note that some ground-based measurements were made about 3 m from the base of the upward-curving blast deflector.

Over the short propagation distances in this measurement (< 23 m) the effects of temperature fluctuations and wind speeds were determined to be minor. Measurements were generally made in the morning and evening to minimize the effects of strong temperature lapses and moderate winds that prevail in the daytime, as well as to minimize temperature effects due to

Fig. 1—The Lockheed Martin/Boeing F-22A Raptor used in the experiment, shown tied down at the HAFB F-22A ground run-up pad. The measurement team members are shown, including personnel from Blue Ridge Research and Consulting, Brigham Young University and Holloman Air Force Base.

increased heating of the fuel during the day. Meteorological trends near the run-up pad were monitored continuously. The average wind speed during the measurements did not exceed 2.4 m/s, except for a single row of scans in plane 2, during which the average wind speed was 5.0 m/s. Temperatures averaged 30°C, with a standard deviation of 4°C. The speed of sound was calculated as a function of temperature, and it was found that the largest fluctuation in sound speed was approximately 6 m/s, or about 2% of the mean sound speed.

A temperature probe was mounted to the field array rig to track temperature fluctuations as a result of the engine firing. It was found that the jet did not heat the ambient fluid significantly within the measurement region. It was therefore determined that any refraction effects due to heating of the air beyond the shear layer were negligible in the measurement region.

2.3   Field Array

The field array used in this experiment (see Fig. 2) allowed for a series of dense, large-aperture, two-dimensional measurements. It was designed and built by Blue Ridge Research and Consulting, and was composed of 90 6.35-mm (0.25-in) GRAS 40BE prepolarized microphones, each coupled with a 26CB
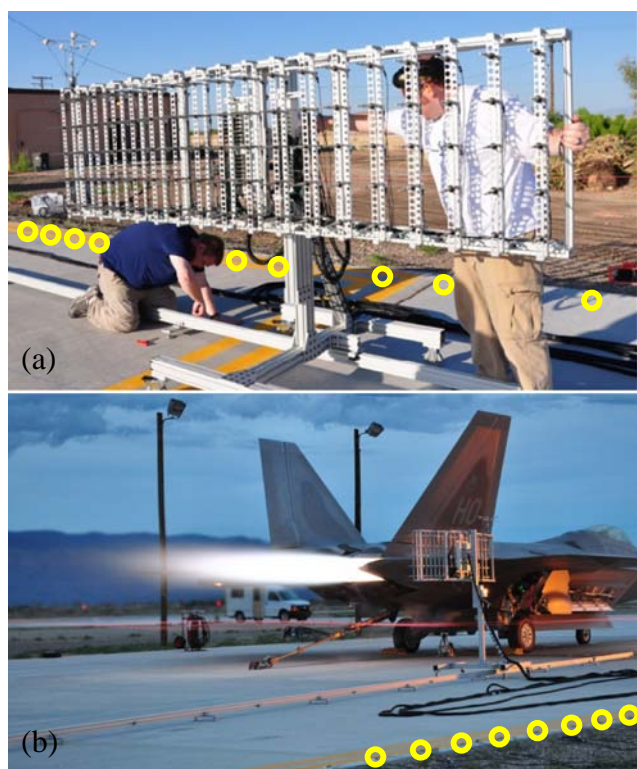

Fig. 2—Two views of the 90-channel field array rig mounted to a guide rail. Reference microphone locations on the ground are marked with yellow circles.
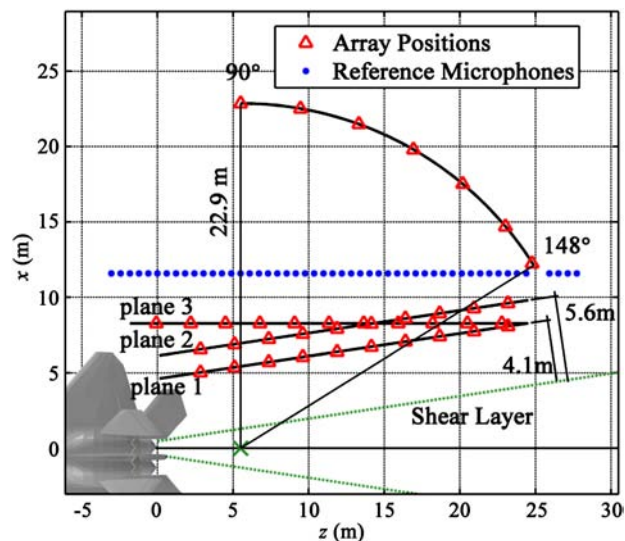

Fig. 3—Schematic of the measurement locations, relative to the aircraft. The estimated shear layer boundary is marked by green dashed lines, and the green "x" delineates the estimated maximum-noise-source region and the center of the arc.

preamplifier, arranged in 5 rows and 18 columns (when in the horizontal orientation) with 0.15-m (6.0-in) equal spacing. The array had an optional horizontal or vertical orientation, an adjustable height, and was mounted to an extruded aluminum guide rail.

Figure 3 describes the field measurement locations relative to the aircraft. In addition to the x and z coordinates marked on the schematic, the vertical axis is represented by y, with a positive direction pointing up. The origin of the coordinate system is on the ground directly below the nozzle exit. Red triangles denote the locations of the field array center for each "scan" (see Sec. 2.6). Planes 1 and 2 were measured parallel to the estimated shear layer boundary, with the array in the horizontal orientation (see Fig. 2), and with the center row at heights of 0.69, 1.29, and 1.91 m (27.0, 51.0, and 75.0 in) above the ground. This provided an overlap of microphone locations, with the microphone locations of the top row overlapping the microphone locations of the bottom row as the rig was raised from 0.69 to 1.29 m, and again from 1.29 to 1.91 m. Plane 3 was measured parallel to the jet centerline, with the array in the horizontal orientation, at heights of 1.29 and 1.91 m. For planes 1–3 the array was moved in 2.3 m (7.5 ft) increments, so that the locations of the first three and last three columns overlapped from scan to scan. All measurement planes were located sufficiently far from the flow to render flow-induced noise negligible.

In addition to the three planar measurements, an arc-shaped surface was measured in the transition region from the near to the far field. The arc was centered at a point 5.5 m (18.0 ft) downstream of the nozzle (marked by a green "x"), with a radius of 22.9 m (75.0 ft). The arc center represents an attempt to approximate the location of the dominant noise source region, although it is understood that this region is noncompact and varies as a function of frequency and engine operating conditions[6]. The location of the arc center and the radius of the arc are consistent with measurement locations used by Gee et al[11] in a previous study of the F-22A Raptor. Measurements were made along the arc at a height of 1.91 m and at six locations in 10° increments from 90° to 140°. A seventh location was measured at 148°, because the edge of the concrete pad made a measurement at 150° difficult. All angles reported in this paper are measured relative to the front of the aircraft (inlet axis) and to the arc center at 5.5 m downstream of the nozzle.

2.4 Fixed-Location Reference Array

An additional 50 microphones (marked by yellow circles in Fig. 2 and by blue dots in Fig. 3) were placed in a fixed-location array to allow for the generation of coherent field measurements from temporally distinct scans, for the purposes of performing near-field acoustical holography. The data recorded at these microphones can be used as reference signals to tie together magnitude and phase discontinuities of the field array from scan to scan, hence the name "reference array." This is done using a process called partial field decomposition, which also compensates for measurement noise and nonstationarity of the jet noise source[3,21]. Although partial field decomposition and holography results are not given here, in this paper the reference array is used to provide overall levels and show spectral variation over a large spatial region in the near field from measurements made simultaneously.

The reference microphones, shown by the blue dots in Fig. 3, were placed on the ground 11.6 m (38.0 ft) from the centerline of the jet in the x-direction (11.7 m total distance in x and y) and spaced 0.61 m (2.0 ft) apart in the z-direction. It was 12.0 m from the center of the aircraft in the x-direction. With references on the ground, multipath interference due to ground reflections was avoided. Several types of microphones were used in the reference array, including GRAS 6.35-mm (0.25-in) 40BD, 40BE and 40BH prepolarized microphones, and GRAS 3.18-mm (0.125-in) 40DD prepolarized microphones. All reference microphones were laid out according to their sensitivities, taking into account the peak sound-pressure levels that were expected along the array.

2.5 Data Acquisition System

The proper design of the data acquisition setup for near-field acoustical measurements of full-scale jet noise is critical. Accurate measurements require the ability to record frequencies that range from the infrasonic to the ultrasonic regimes, and to capture data over a very large spatial aperture and dynamic range. For example, the field array was restricted to distances beyond 4.1 m, where instantaneous sound pressure levels (SPLs) exceeded 170 dB re 20 µPa. This converts to an approximately 6.3 V signal peak for a nominal rig-microphone sensitivity of 1 mV/Pa. (Some of the field array microphones had a sensitivity as high as 1.28 mV/Pa.) With these requirements in mind, a National Instruments (NI) PXI-1045 chassis system with NI PXI-4498 and NI PXI-4462 cards served as the A/D converters, which streamed data to an NI 8353 rackmount controller with a high-power Intel Core 2 Quad processor and four 250-GB hard drives in a RAID-0 configuration. The entire data acquisition system was monitored using a laptop with a Windows Remote Desktop, which allowed for wireless or wired connection to the controller. The software was a custom designed LabVIEW data acquisition program, which provided setup, microphone calibration, real-time level and spectral monitoring and channel overload alerts. BNC cables ran from the microphones to several NI BNC-2144 InfiniBand-to-BNC breakout boxes. Then bundled InfiniBand cables ran from the breakout boxes to the NI PXI cards. This setup allowed for the simultaneous measurement of 150 channels. The data acquisition setup is pictured in Fig. 4.
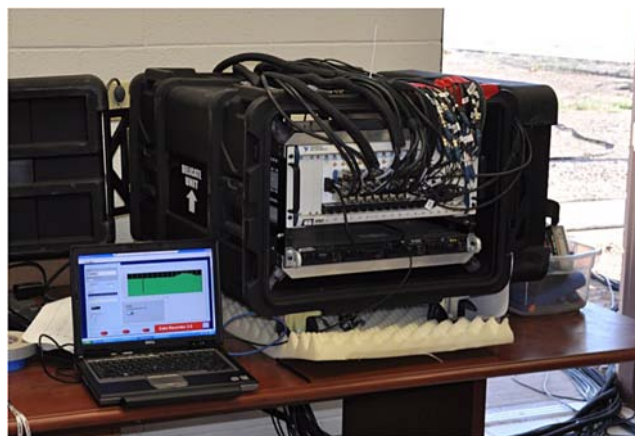

Fig. 4—Laptop, NI PXI-1045 chassis, and NI 8353 rackmount controller used for data acquisition. The chassis and controller are mounted in a shock mount rack case, and the entire system is in a building located near the run-up pad.

During afterburner conditions, several reference-array channels centered around $100°$, corresponding to microphones with the highest sensitivities, experienced infrequent capacitive-like effects in the time waveform. Further investigation has shown that this effect is due to insufficient response time of the on-board constant-current supplies when very rapid rises (i.e., steep shocks) occurred in the pressure field. These capacitive effects, which were manifest as low-frequency spectral noise, were removed from the time waveform data prior to processing. Recommendations for avoiding these effects in future jet and rocket noise measurements are provided by Taylor et al[22].

Careful vibration isolation measures are necessary for data acquisition systems used during high-power jet noise measurements. In this experiment, while the aircraft engine operated at afterburner conditions, high-amplitude, acoustically induced vibrations caused the hard drives to stop writing temporarily. This caused the on-board memory buffer to fill before writing all the data to disk, precluding the 96-kHz sampling frequency used for lower engine powers. In an attempt to address the problem, the data acquisition system was placed in a nearby building and mounted in a shock-mount rack case, seen in Fig. 4. These measures, however, were insufficient, particularly because the energy of the acoustic signatures was dominated by low frequencies (~ 100 Hz). An accelerometer placed directly on the rackmount controller measured rms acceleration values of 1.58 m/s^2 during afterburner conditions. To work around the problem, during afterburner engine firings the measurements were recorded at a sampling frequency of 48 kHz instead of the 96 kHz used for all other conditions. The lower sampling frequency caused the buffer to fill more slowly, allowing it time to write all the data to disk. In future measurements, a solid-state hard drive or more robust vibration isolation methods are recommended.

2.6 Test Sequence

Before testing, the aircraft was tied down to the run-up pad, the reference microphones were attached in place, the field array was mounted to the guide rail in the horizontal position and at the desired distance from the jet (see Fig. 2), and all channels were calibrated and deemed functional. Then, when the meteorological conditions were suitable (as described in Sec. 2.2), the measurements began. The aircraft engine was fired to operate on condition at idle power, and the pilot signaled the measurement team by rotating the horizontal stabilizers on the rear of the aircraft. Then pressure waveforms were recorded by all microphones at a sampling frequency of 96 kHz for 30 s. When the

measurement was complete, a member of the team signaled the pilot to go to intermediate engine conditions. With the engine on condition, the measurement process was repeated. Military engine conditions were recorded in the same manner. Then the sampling frequency setting of the data recorder software was decreased to 48 kHz. At this lower sampling frequency the measurement was performed for afterburner engine conditions. The aircraft engines were then returned to idle conditions, the sampling frequency setting was returned to 96 kHz, and two team members moved the field array to the subsequent measurement position. When all measurement scans were taken in a row along the length of the jet (with the array at a fixed height and offset distance), the aircraft was powered down for cooling and the addition of fuel, while the height of the array or its offset distance was changed.

The sequence of cycling through each of the four engine conditions and recording data with the field array and reference microphones in a single fixed location is referred to as a "scan". Scan locations of the field array are marked by red triangles in Fig. 3. Each measurement plane shown in Fig. 3 was composed of a set of scans made along the length of the jet and at several heights. The resulting database after all measurements were performed was approximately 650 GB in size.

3 RESULTS AND DISCUSSION

This section presents several results of the near-field experiment described above, with an emphasis on level-based analyses. Specifically, acoustically induced vibrations of the rig, OASPLs, spectral content and the variation of the spectra over space, sound-field stationarity and characteristics of time waveforms are examined for subsets of the data. In each subsection, measurement results are presented followed by a discussion of the corresponding physical phenomena that are important for understanding full-scale jet noise.

3.1 Vibration Measurements

Before showing measured results, it is important to establish the quality of data taken on the rig. Specifically, it is shown that rig vibrations did not appreciably affect measured quantities. Acoustically induced vibrations of the rig led directly to vibrations of the microphones, which increased their effective noise background. Euler's equation, which relates a pressure gradient to particle acceleration, can be used to link the microphone motion directly to a theoretical, false pressure wave. If it is assumed that a time-harmonic plane wave is incident on the microphone diaphragm, then from Euler's equation the false pressure

magnitude as a function of frequency is related to the microphone acceleration by

$$|p(f)| = \left| \frac{\rho_0 ca(f)}{2\pi f} \right| \qquad (1)$$

where $p(f)$ is the false pressure in Pa, f is the frequency in Hz, ρ_0 is the ambient air density, c is the ambient sound speed and $a(f)$ is the acceleration of the microphone in m/s^2. In this formulation it is assumed that the vibration measured by the accelerometer is representative of the vibration of the diaphragm of the nearby microphone (i.e. there was a rigid connection from the rig to the diaphragm).

Accelerometers were placed in several locations on the rig frame during engine run-ups to measure microphone accelerations (along the microphone axis). The data shown are for a microphone within 8 cm of the accelerometer. Using Eqn. (1) the measured accelerations were converted to false SPLs and compared to the measured SPLs of the nearby microphone. Figure 5 shows the measured and false SPLs (in one-third octave band bins) in the case when the rig was at a height of 1.91 m, on plane 2 and in the region of maximum
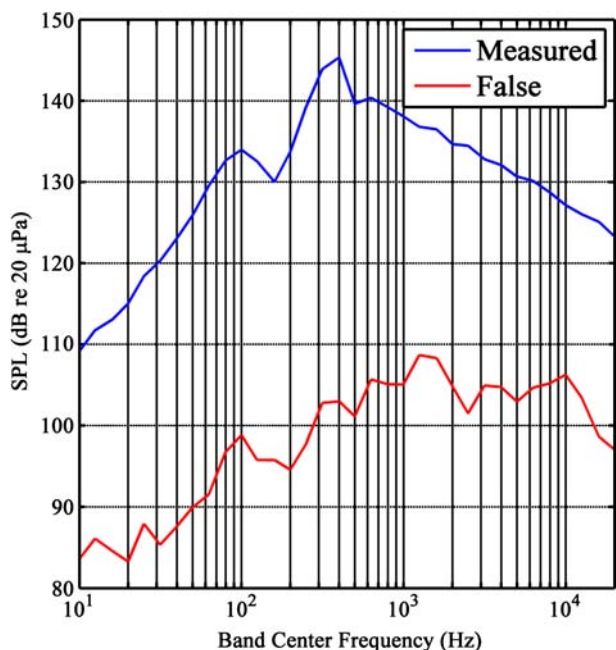

Fig. 5—One-third octave band SPLs measured by a microphone on the rig, located at z = 9.6 m downstream on the top row of plane 2, with the engine operating at afterburner conditions. Also shown is the corresponding false SPL calculated from acceleration measurements by an accelerometer located near the microphone.

radiation ($z = 9.6$ m engine downstream) for afterburner conditions. The resulting theoretical noise background ranges from about 20 to 40 dB below the actual measured SPLs over all frequencies of interest. For most engine conditions, frequencies, and locations in the field the theoretical noise background, derived from rig vibrations, are at least 20 dB below the measured SPLs. At idle and intermediate conditions the false SPLs produced approach the measured levels above 10 kHz in several instances, but these frequencies are already ignored in this paper because they contain noise components (see Sec. 3.3.1). Hence, rig vibrations do not play a significant role in the measured acoustic quantities reported through the remainder of Sec. 3.

3.2   Overall Sound Pressure Levels

In order to characterize the aircraft maintainer environment the OASPLs over the measured spatial aperture are given. Important clues about jet-noise radiation characteristics can be obtained by observing the change in overall radiation patterns as a function of engine condition. Figures 6 and 7 show OASPLs measured by the field array for military and afterburner engine conditions, respectively. Both figures have a color scale that spans 20 dB. Note that Gee et al[11] measured OASPLs for the F-22A Raptor on the same arc as that shown here (23 m from the arc center). At a height of 1.8 m and at 125°, the OASPL they measured for afterburner conditions was 143 dB re 20 µPa, which agrees to within 1 dB of the measured value shown in Fig. 7.

The OASPLs measured by the reference microphones, averaged over several scans, for all four engine power conditions are shown in Fig. 8. The directly measured levels, represented by black dots, show a somewhat "noisy" variation in level along the reference array. These local variations are a result of a slight bias in the field-calibrated microphone sensitivities. They are greater for the 3.18 mm microphones (located between z values of 12.2 and 16.5 m), which had the lowest sensitivities (0.2–0.4 mV/Pa) and are the most difficult to calibrate in the field. To correct for this uncertainty in calibration, a set of weighting factors was derived by visual inspection of the variation in the levels of the intermediate case. The intermediate condition was chosen because it has the flattest spatial distribution. These resulting factors were then applied to all scans and engine conditions, and the resulting "filtered" results are represented by the solid lines. (The dashed lines represent ± 1 standard deviation of the OASPL at each location and are used to explore the stationarity of the source from scan to scan in Sec. 3.2.2).

The reference microphone array, placed along the ground at a perpendicular distance of 12.0 m (39.5 ft) from the center of the aircraft, was near the 42-ft "foul
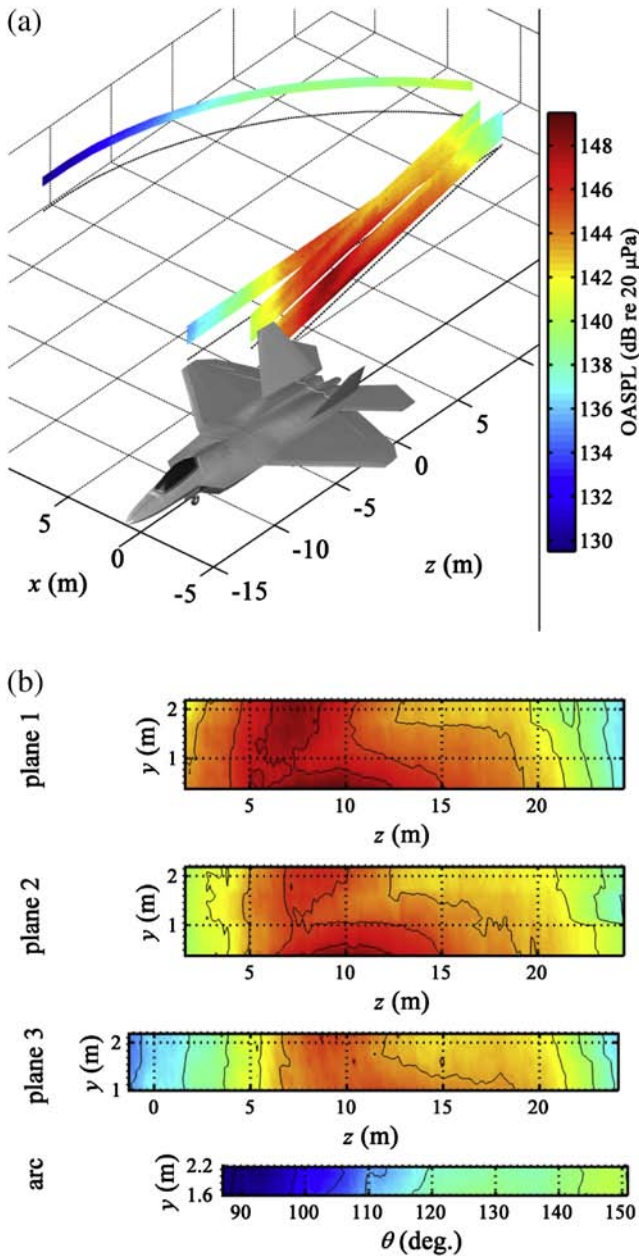
Fig. 6—OASPLs measured in the geometric near field at military engine conditions. (a) Levels are plotted at their three-dimensional locations. (b) Levels of measurement planes 1–3 are projected onto the z–y plane; levels of the measurement arc are plotted as a function of polar angle.

line" position where aircraft maintainer personnel often stand in relation to the jet on the deck of an aircraft carrier. Figure 8 shows that, at afterburner conditions, there is a 25-m region where the OASPL exceeds 140 dB re 20 μPa, and a 5-m region where the OASPL exceeds 150 dB re 20 μPa. The levels at the head of an aircraft maintainer are expected to be slightly lower,

since the measurements here experienced a level boost due to the ground reflection, and were taken 0.76 m closer to the jet than the foul line position. Also note that the OASPL difference between military and afterburner conditions ranges from about 5 to 6 dB over most of the measurement aperture ($z \leq 19$ m).

The relative locations of maximum-level regions from one measurement plane to the next, shown in
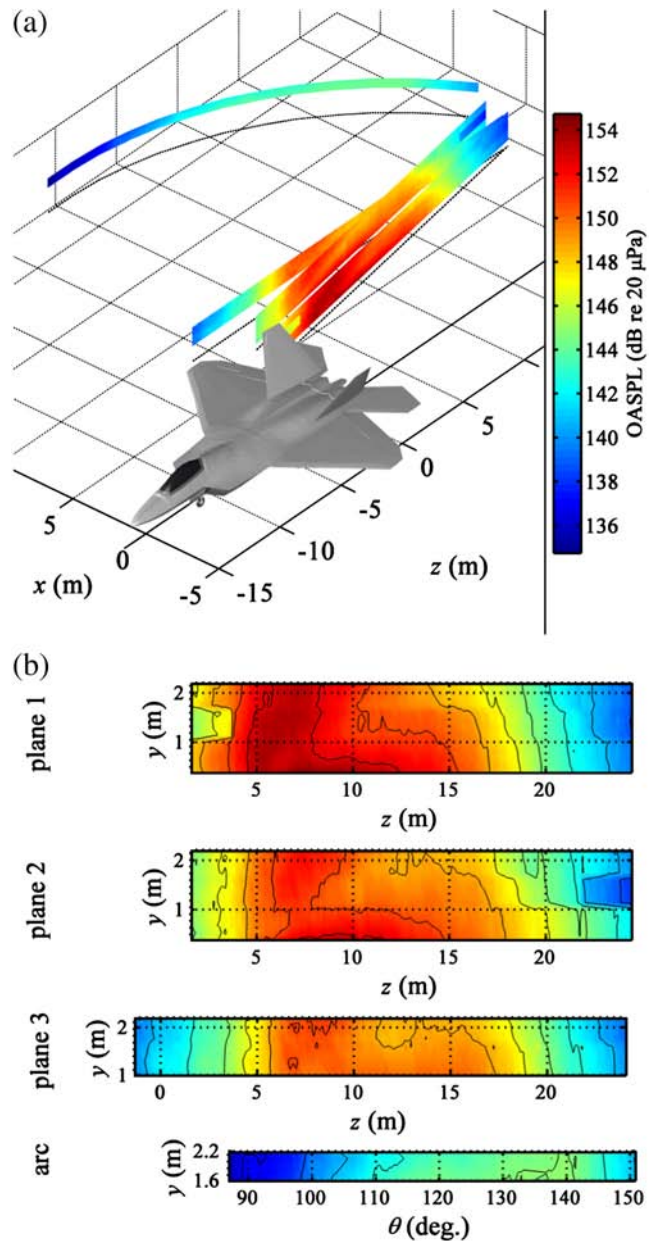

Fig. 7—OASPLs measured in the geometric near field at afterburner engine conditions. (a) Levels are plotted at their three-dimensional locations. (b) Levels of measurement planes 1–3 are projected onto the z–y plane; levels of the measurement arc are plotted as a function of polar angle.
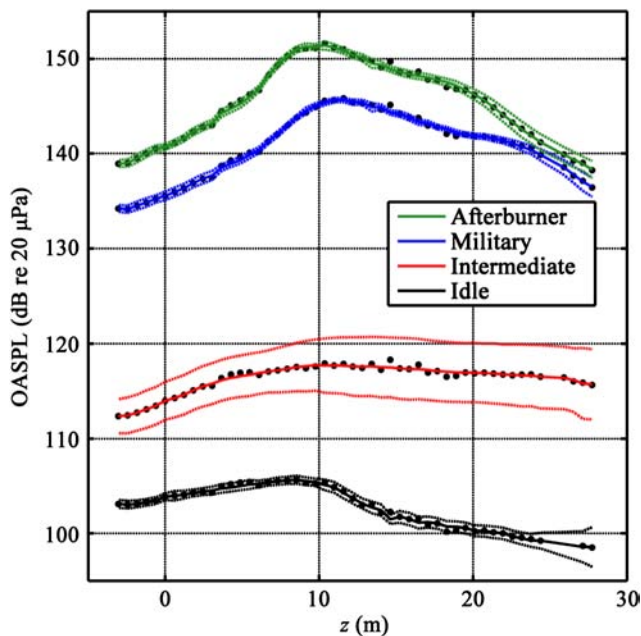
Fig. 8—OASPLs measured along the ground 12.0 m from the jet centerline by the reference array, for all engine power conditions. Black dots indicate averages of directly measured values and exhibit slight spatial noise due to microphone-sensitivity biases. Smoothed data are shown by a solid colored line, and ± 1 standard deviation over all scans is represented by colored dashed lines.

Figs. 6(a) and 7(a), as well as the distinct maximum-level regions in Fig. 8, demonstrate a strong lobing of the overall radiation in the aft direction for military and afterburner conditions. However, two important distinctions between military and afterburner conditions exist in the results. The first is that the maximum region measured along the reference array in Fig. 8 shifts forward 2 or 3 m as engine condition increases from military to afterburner. This corresponds to a forward shift of about 10° and is likely due to an increase in the convective speed of large-scale turbulence structures (see Figs. 2.2.9 and 2.2.10 in Ref. 23).

The second distinction is that the high-amplitude sound-field region within the measurement aperture for afterburner conditions is more spatially compact than that for military conditions. Since the measurement aperture is limited to the near field, the exact differences in the principal radiation lobes are unclear. Certainly, a simple difference in how the measurement planes "slice through" two different lobes of similar shape but different orientation would alter the spatial extent of a maximum region. It is also possible that a

change in the nature of the source could lead to a narrower principal lobe at afterburner conditions than at military, but a rigorous directivity analysis is precluded here by the lack of concurrent far-field data.

3.3 Spectral Analysis

Turbulent structures within a jet vary greatly in their length and time scales. This manifests itself in the broadband spectra of measured jet noise. In this subsection an examination of the measured spectra, an assessment of the sound field stationarity and a spatial/spectral analysis of the near field radiation lead to insights regarding the frequency dependence of jet noise.

3.3.1 Spectral content

The spectral content in the near field is represented here by the frequency-dependent sound pressure levels (SPLs) measured for all four engine conditions at two key locations within the field. The first, at $z = 5.5$ m downstream (corresponding to an angle of 90° with respect to the front of the aircraft) is shown in Fig. 9, and a second at $z = 15.2$ m downstream (corresponding to 130°) is shown in Fig. 10. These locations are important because previous studies often indicate that jet noise is composed of two distinct source components: fine-scale turbulence that dominates the sideline radiation, and large-scale turbulence structures that dominate the downstream radiation[24,25]. The one-third octave SPLs represented by solid lines in Figs. 9 and 10 have been averaged over all scans. The dashed lines show ± 1 standard deviation of the SPLs at each frequency and engine condition, and are used to assess stationarity in Sec. 3.2.2. Data for the upper frequencies of the idle and intermediate conditions are not included because they are contaminated by engine noise components. The legends of Figs. 9 and 10 list the mean values and standard deviations of the OASPLs corresponding to each condition. Note that there is significant spectral energy below 10 Hz and above 20 kHz at some conditions, reaffirming the need for broadband data acquisition and instrumentation capabilities.

A comparison of Figs. 9 and 10 indicates that the higher frequencies tend to dominate the noise to the sideline, while lower frequencies dominate in the downstream direction. For example, at $z = 5.5$ m downstream the maximum frequencies are within the 400-Hz one-third octave band for intermediate engine conditions, the 630-Hz band for military conditions, and the 800-Hz band for afterburner conditions. However, at $z = 15.2$ m, the maximum-frequency bands are 100 Hz for intermediate, 250 Hz for military, and 125 Hz for afterburner conditions. Note that the spectra for idle engine power at both locations do not have
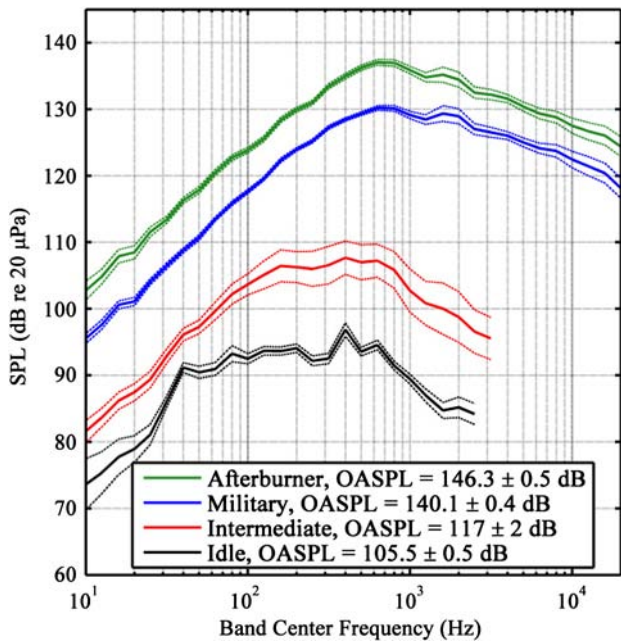
Fig. 9—*One-third octave spectra measured along the reference array at z = 5.5 m downstream (90°). Solid lines represent SPL values averaged over all scans. Dashed lines represent ± 1 standard deviation. The legend includes the mean values and standard deviations of the respective OASPLs. The upper frequencies of idle and intermediate are not shown due to engine-noise components.*

a well defined of a characteristic "haystack" shape; hence it is more difficult to draw conclusions about the dependence of dominant frequencies on location with these data.

The spectral dependence on location is qualitatively consistent with the popular two-source jet-noise model. Schlinker[4] and Laufer et al[24] were the first to observe that there are two independent sources of jet noise: one source generated by large-scale turbulent structures that radiates preferentially in the aft direction and generates Mach waves, and a source generated by the fine-scale turbulence that dominates to the sideline of the jet. Tam et al[25,26] developed empirically determined similarity spectra to characterize the noise radiated by these two sources for any jet. The application of the two-source similarity spectra to high-power jet noise is under investigation[27].

It is interesting to compare the spectral shapes shown in Fig. 10 for military and afterburner engine conditions measured at z = 15.2 m. With the increase in power from military to afterburner, high frequencies are boosted by about 3 dB, while low frequencies are

boosted by about 8 dB. This is accompanied by a double-peak near the dominant frequencies. The double-peak is not found in laboratory-scale jet noise, but is observed in other full-scale jet ground run-up measurements[11,14,28]. The lower-frequency spectral peak might, in part, be due to the impingement of the jet flow on the ground as it expands downstream of the nozzle, which is referred to as "scrubbing"[29]. However, Greska and Krothapalli[13] show a double-peak in the spectrum of an F404-GE-402 jet engine mounted 5.5 m above the ground, which virtually eliminated scrubbing effects. Evidence of a double-peak also appears in flyover measurements of the F-15 ACTIVE Aircraft[30] and in flyover measurements of a military jet by McInerny et al[31]. The presence of this feature in full-scale jet noise merits further study.

3.3.2 Sound field stationarity

To create accurate representations of the sound field over the large measurement planes described in Fig. 3,
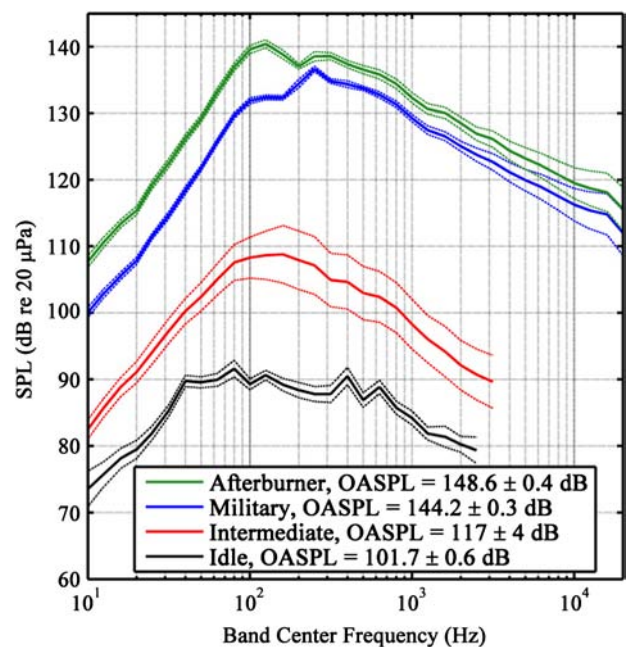

Fig. 10—*One-third octave spectra measured along the reference array at z = 15.2 m downstream (130°). Solid lines represent SPL values averaged over all scans. Dashed lines represent ± 1 standard deviation. The legend includes the mean values and standard deviations of the respective OASPLs. The upper frequencies of idle and intermediate are not shown due to engine-noise components.*
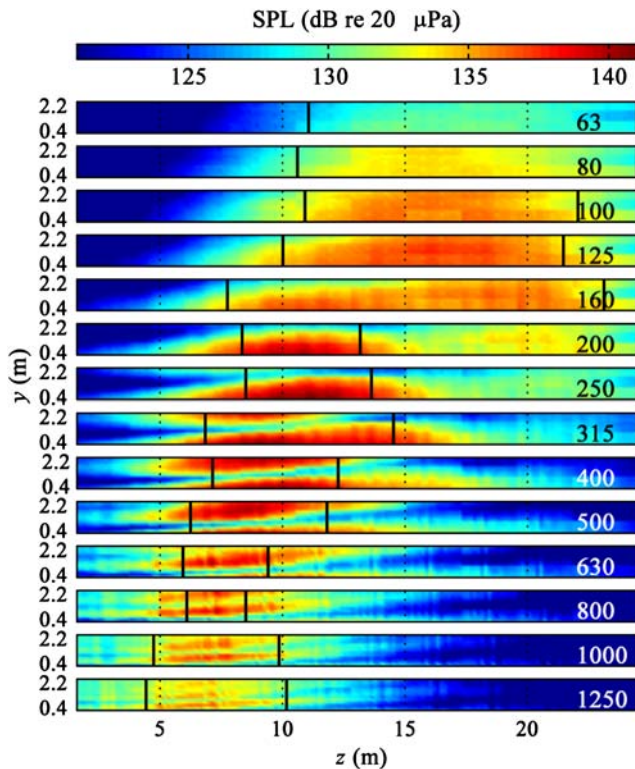
Fig. 11—SPLs measured at plane 2 for several one-third octave bands at military engine power conditions. Vertical black lines indicate the regions where SPLs are within 3 dB of the maximum SPL. The number at the right of each plot is the band center frequency in Hz.

about 0.3 dB for idle, military, and afterburner conditions. However, the levels in the extreme aft locations varied by as much as 1 dB. The effects of this aft fluctuation may also be seen in the highly discontinuous scans at the right in Figs. 6 and 7. Possible causes for this greater variability include wave propagation in the near-axial direction through fluctuating turbulent flow, a particularly strong variation in the sources that radiate in the far aft direction, scrubbing of the flow on the ground, or interference by the blast deflector. Recall that the reference microphone farthest downstream was located about 3 m from the bottom of the deflector. The lower stationarity in this region requires further investigation.

3.3.3 Spatial/band-level maps

The spectral variation along the rig planes and the reference array may be used to indirectly infer source characteristics. First, Figs. 11 and 12 show SPL maps of several one-third octave bands measured using the field array at plane 2 (see Fig. 3). Figure 11 contains
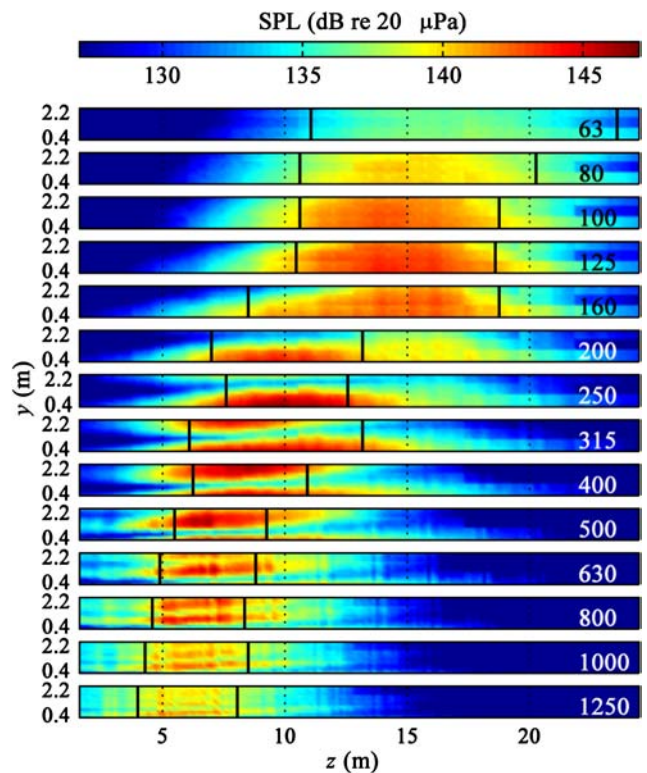

Fig. 12—SPLs measured at plane 2 for several one-third octave bands at afterburner engine power conditions. Vertical black lines indicate the regions where SPLs are within 3 dB of the maximum SPL. The number at the right of each plot is the band center frequency in Hz.

it is important to determine stationarity of the noise field produced for each engine run-up. Consequently, frequency and spatial-based stationarity evaluations are performed here to determine how consistent the measurements were from scan to scan. To address stationarity of the sound field for each frequency, the ± 1 standard deviation values of the one-third octave SPLs were calculated for all four engine conditions and are shown as the dashed lines in Figs. 9 and 10. For most engine operating conditions and frequencies below about 3 kHz the standard deviations from scan to scan of the power spectra were less than 1 dB, and were less than 2 dB below 10 kHz. Intermediate engine conditions were less consistent than other conditions because there is no "intermediate" set throttle position for the F-22A as there is for the other conditions.

The stationarity of the sound field over space was evaluated by including the standard deviations of the reference array-measured OASPLs in Fig. 8, also as dashed lines. The OASPL standard deviations measured at most reference microphones were less than
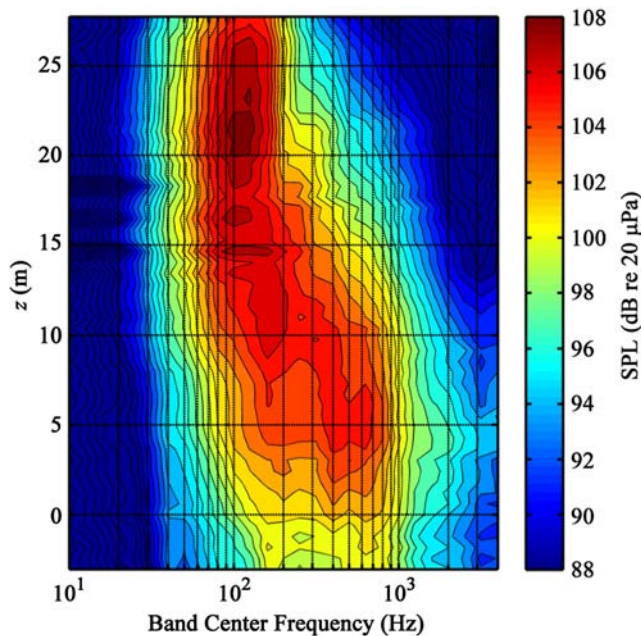
Fig. 13—One-third octave spectral variation over location along reference array at intermediate engine conditions. Each contour line represents a step size of 1 dB.

the SPLs measured at military engine power, and Fig. 12 displays afterburner conditions. The corresponding one-third octave band center frequency in Hertz is displayed in the bottom right corner of each map. A color axis that spans 20 dB is used in each map for consistency. Vertical black lines in both figures mark the edges of the regions where all SPLs in the column drop at least 3 dB below the maximum SPL. Note that the variability of the field for intermediate engine conditions (see Figs. 8 through 10) reduces the utility of similar maps for that engine power.

Before proceeding to level-based maps for the reference array, some comments about what is readily learned from Figs. 11 and 12 are merited. First, as is characteristic of jet noise, both the maps for military and afterburner show that the maximum-level region (demarcated by the 3-dB down points) moves upstream and generally becomes more compact as frequency increases. Second, there is also some indication that the location of this dominant region is asymptotically approaching some limit downstream of the nozzle for these conditions. This is supported by the level maps of higher frequencies (not shown). Although this is a field measurement rather than a source measurement, the upstream movement and spatial constriction of the maximum-level region with increasing frequency agrees, in principle, with Lee and Bridge's[7] phased-array estimates of the dominant aeroacoustic source region in heated model-scale jets.

The rig-based SPL maps in Figs. 11 and 12 contain horizontal null regions due to multipath interference effects from reflections off the run-up pad. Although these interference nulls are present in realistic run-up and take-off environments, and can be useful in understanding source characterisics[32,33], the additional spatial variation of spectral levels due to the presence of a reflecting plane can make examination of spectral trends more difficult. Therefore, there it is useful to examine level-based maps measured by the reference array, which was placed on the ground. SPLs as a function of one-third octave band-center frequency and location in z are displayed in Figs. 13 through 15 for intermediate, military, and afterburner engine conditions, respectively. The contour lines represent step sizes of 1 dB, and all color axes span a range of 20 dB.

Figures 13 through 15 reveal the trend that the region of maximum level in the near field moves upstream and constricts spatially with an increase in frequency for all three engine conditions. They also demonstrate further the two-peak phenomenon seen at afterburner and military powers in Fig. 10 (the data shown in Fig. 10 could be considered "slices" through Figs. 13 through 15 at $z = 15.2$ m). In Figs. 14 and 15, there appear to be two distinct, dominant, spatio/spectral components, or regions of local maximum level. The high-frequency component dominates farther upstream and the low-frequency component dominates in the downstream direction. For the afterburner conditions shown in
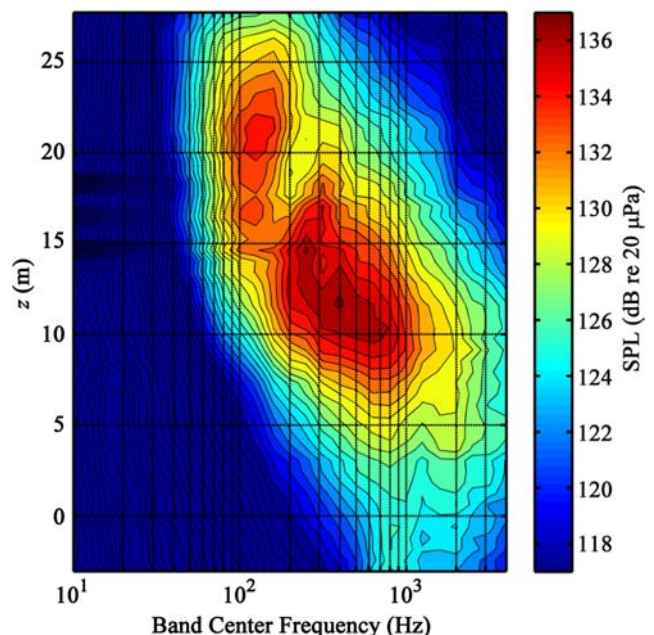

Fig. 14—One-third octave spectral variation over location along reference array at military engine conditions. Each contour line represents a step size of 1 dB.

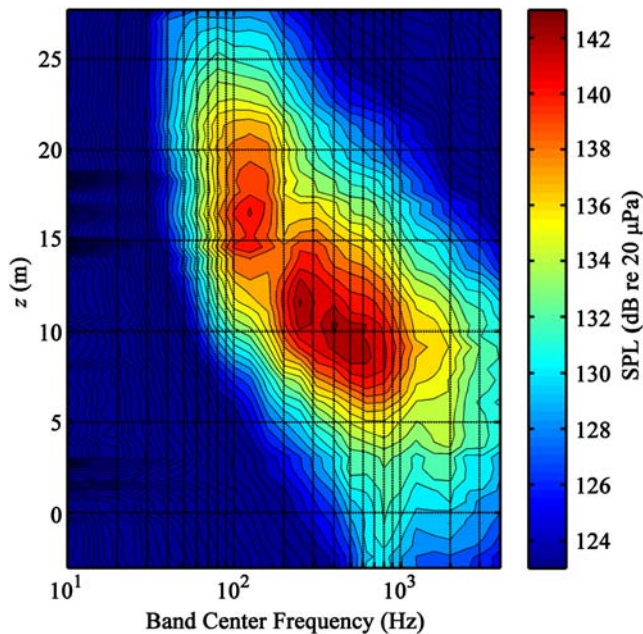Noise Control Engr. J. **60** (4), July-August 2012

431

Fig. 15—One-third octave spectral variation over location along reference array at afterburner engine conditions. Each contour line represents a step size of 1 dB.

Fig. 15, the spectra between $z = 13$ m and $z = 22$ m all contain a local maximum frequency near 125 Hz. However, the local frequency maxima of the second component are spatially dependent. Near $z = 14$ m the dominant frequency is about 250 Hz, but shifts gradually to 800 Hz near $z = 5$ m. The results of military conditions are qualitatively similar in Fig. 14, and although the distinction between two peaks does not occur in the intermediate case (see Fig. 13), there is a downstream region where the dominant frequencies (near 160 Hz) do not depend on z, and a region upstream where the dominant frequency is spatially dependent.

Caution should be used in drawing conclusions about far-field directivity from the spatial maps in Figs. 8 and 11 through 15, since the measurements were taken in the geometric near field. For example, note that the farthest-aft portion of the arc is only about 8 m from the estimated shear layer location. In addition, although the features are similar, when the angular locations of either the arc or the reference microphones are used, similar features for the afterburner spectra are farther aft by 5-10° relative to far-field F-22A spectra shown previously by Gee et al[11].

3.4 Time Waveforms

An examination of directly recorded time waveforms reveals the presence of acoustic shocks and helps to explain important spectral characteristics. Figure 16 shows pressure waveform data measured at $z = 5.5$ m

on the reference array for all engine conditions, and Fig. 17 shows waveforms measured at $z = 15.2$ m. These are the same respective locations for which the spectra are plotted in Figs. 9 and 10. For each waveform, the peak amplitude of the entire 30 s time record is shifted to the 10 ms position. Note the presence of shocks in both the sideline and downstream directions for military and afterburner conditions.

An important difference between the sideline and downstream jet noise may be observed by comparing the waveforms shown in Figs. 16 and 17 for each engine condition individually. The waveforms in the downstream location, for both military and afterburner conditions, are broader in time and have fewer zero crossings than those measured to the side. This accounts for the spectral maxima occurring at lower frequencies in Fig. 10 than those given in Fig. 9. A likely reason for this is that the sideline radiation is dominated by noise from the fine-scale turbulence structures, which are inherently higher in frequency to begin with, while the aft measurement is dominated by directional noise from large-scale structures[25,26].

Acoustic shock structures with sharp rise times are present in both the military and afterburner waveforms to the sideline (see Figs. 16(c) and (d)) and in the downstream direction (see Figs. 17(c) and (d)). The formation of shocks due to nonlinear propagation induces a shift of spectral energy toward higher frequencies[11,28]. The presence of shocks in the near field[14,27,34] requires further investigation.

3.5 Crest Factor

The crest factor, or the difference between peak and rms overall levels, is an essential measure when
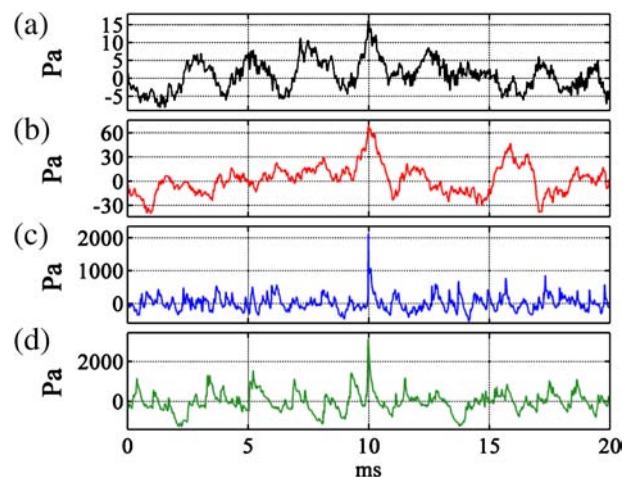

Fig. 16—Pressure waveforms measured at z values of 5.5 m (90°) for (a) idle, (b) intermediate, (c) military and (d) afterburner engine conditions.

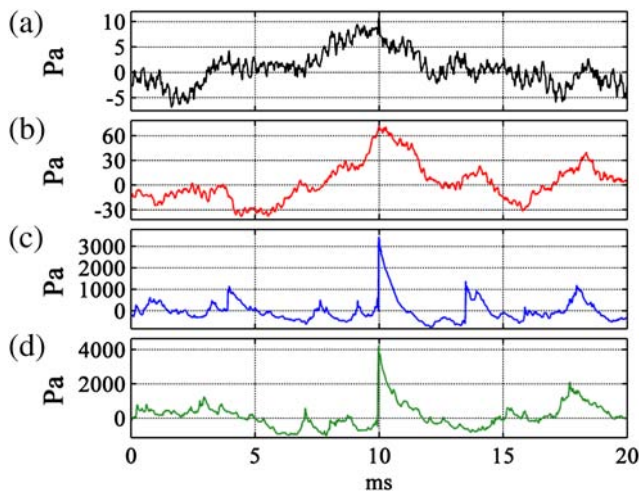*Fig. 17—Pressure waveforms measured at z values of 15.2 m (130°) for (a) idle, (b) intermediate, (c) military and (d) afterburner engine conditions.*

designing a high-amplitude jet noise measurement. Not only must measurements be made over a large dynamic range, it is the peak pressures, rather than the rms pressures, that limit the proximity of microphones to the jet. In this analysis, the crest factor was found along both the rig and reference arrays as a function of engine condition and location. A 99.999[th] percentile criterion was used; i.e., 99.999% of all instantaneous pressure amplitudes in a waveform were below the peak value found. This essentially corresponds to one pressure value above the calculated peak value every 2 s at afterburner conditions, or every 1 s at other conditions.

The largest peak pressure measured on the array at plane 1 for afterburner conditions was 6443 Pa (170 dB re 20 μPa). The corresponding crest factor was 16.7 dB. Peak pressures at the reference array (which was placed on the ground to avoid multi-path interference but, therefore, experienced a pressure boost) for afterburner engine conditions reached 6183 Pa (170 dB re 20 μPa). The crest factor at this location was 18.1 dB. Both maximum crest factor estimates agree with previous works by statement by Gabrielson et al[34] and by McInerny[35] that peak pressures can be five to ten times (or 14–20 dB) greater than rms pressures for high-power aeroacoustic noise. This information should prove useful in the future design of near-field experiments on full-scale jet noise.

4   CONCLUSIONS

Turbulent jets from full-scale engines on military aircraft are some of the largest and most complicated noise sources of interest in aeroacoustics. Near-field experiments on these sources require measurements to be made over tens of meters in length, for noise over a very large dynamic range and with significant spectral content from the infrasonic to the ultrasonic regimes. This paper describes basic results of measurements made in the geometric near field of the jet on an F-22A Raptor. It is shown here that an increase in engine power from military to afterburner conditions results in a forward-shifting of the noise radiation and a possible increased lobing effect. It is also shown that, in the downstream direction, as engine power increases from military to afterburner engine conditions the low-frequency noise components increase much more rapidly than high-frequency components. This is coupled with the occurrence of two distinct maximum regions in the level maps as a function of frequency and location: a low-frequency component that dominates downstream and where the maximum frequency is nearly independent of location, and a high-frequency component that dominates upstream with a location-dependent maximum frequency. It is also shown that the noise measured in the far downstream locations is less stationary than the noise measured elsewhere.

The scope of the measurements made in this experiment provides for a detailed characterization of full-scale jet-noise sources and the near sound field using near-field acoustical holography methods. The extensive measurements should also allow for future beamforming, near-field correlation and coherence, vector acoustic intensity, partial field decomposition and nonlinear propagation analyses. These analyses can expand the understanding of high-power jet noise properties in the near field and help to determine important jet-noise source characteristics.

5   ACKNOWLEDGMENTS

Noise Control Engr. J. **60** (4), July-August 2012

433

6 REFERENCES

1. M.M. James, K.L. Gee, A.T. Wall, J.M. Downing, K.A. Bradley and S.A. McInerny, "Aircraft jet source noise measurements of a Lockheed Martin F-22 fighter jet using a prototype near-field acoustical holography measurement system", *J. Acoust. Soc. Am.*, **127**(3), 1878, (2010).

2. M.M. James and K.L. Gee, "Aircraft Jet Plume Source Noise Mesurement System", *Sound Vibr.*, **44**(8), 14–17, (2010).

3. A.T. Wall, K.L. Gee, M.D. Gardner, T.B. Neilsen and M.M. James, "Near-field acoustical holography applied to high-performance jet aircraft noise", *Proceeedings of Meetings in Acoustics (POMA)*, **9**(1), 040009, (2011).

4. R.H. Schlinker, "Supersonic Jet Noise Experiments", Ph.D. Dissertation, University of Southern California, Los Angeles, CA, (1975).

5. C.K.W. Tam, "Supersonic jet noise", *Annu. Rev. Fluid Mech.*, **27**(1), 17–43, (1995).

6. C.K.W. Tam, N.N. Pastouchenko and R.H. Schlinker, "Noise source distribution in supersonic jets", *J. Sound Vibr.*, **291**(1–2), 192–201, (2006).

7. S.S. Lee and J. Bridges, "Phased-Array Measurements of Single Flow Hot Jets", AIAA Paper 2005–2842, (2005).

8. J.C. Yu and D.S. Dosanjh, "Noise Field of a Supersonic Mach 1.5 Cold Model Jet", *J. Acoust. Soc. Am.*, **51**(5A), 1400–1410, (1972).

9. R. Reba, J. Simonich and R. Schlinker, "Measurement of Source Wave-Packets in High-Speed Jets and Connection to Far-Field Sound", AIAA Paper 2008–2891, (2008).

10. T. Suzuki and T. Colonius, "Instability waves in a subsonic round jet detected using a near-field phased microphone array", *J. Fluid Mech.*, **565**, 197–226, (2006).

11. K.L. Gee, V.W. Sparrow, M.M. James, J.M. Downing, C.M. Hobbs, T.B. Gabrielson and A.A. Atchley, "The role of nonlinear effects in the propagation of noise from high-power jet aircraft", *J. Acoust. Soc. Am.*, **123**(6), 4082–4093, (2008).

12. K. Viswanathan, "Does a Model-Scale Nozzle Emit the Same Jet Noise as a Jet Engine?", *AIAA J.*, **46**(2), 1715–1737, (2008).

13. B. Greska and A. Krothapalli, "On the Far-Field Propagation of High-Speed Jet Noise", *NoiseCon08*, (2008).

14. R.H. Schlinker, S.A. Liljenberg, D.R. Polak, K.A. Post, C.T. Chipman and A.M. Stern, "Supersonic Jet Noise Source Characteristics & Propagation: Engine and Model Scale", AIAA Paper 2007-3623, (2007).

15. M. Lee and J.S. Bolton, "Source characterization of a subsonic jet by using near-field acoustical holography", *J. Acoust. Soc. Am.*, **121**(2), 967–977, (2007).

16. A.T. Wall, K.L. Gee, M.M. James and M.D. Gardner, "Application of near-field acoustical holography to high-performance jet aircraft noise", *J. Acoust. Soc. Am.*, **127**(3), 1879, (2010).

17. A.T. Wall, K.L. Gee, T.B. Neilsen and M.M. James, "Considerations for near-field acoustical inverse measurements on partially correlated sources", *J. Acoust. Soc. Am.*, **128**(4), 2285, (2010).

18. H. Vold, P.N. Shah, J. Davis, P.G. Bremner, D. McLaughlin, P. Morris, J. Veltin and R. McKinley, "High-resolution continuous scan acoustical holography applied to high-speed jet noise", AIAA Paper 2010-3754, (2010).

19. C.K.W. Tam, "Influence of Nozzle Geometry on the Noise of High-Speed Jets", *AIAA J.*, **36**(8), 1396–1400, (1998).

20. T.J.S. Jothi and K. Srinivasan, "Acoustic Characteristics of Non-Circular Slot Jets", *Acta Acustica united with Acustica*, **94**(2), 229–242, (2008).

21. M. Lee and J.S. Bolton, "Scan-based near-field acoustical holography and partial field decomposition in the presence of noise and source level variation", *J. Acoust. Soc. Am.*, **119**(1), 382–393, (2006).

22. R.T. Taylor, K.L. Gee, J.H. Giraud, S.D. Sommerfeldt, J.D. Blotter and C.P. Wiederhold, "On the use of prepolarized microphones in rocket noise measurements", *J. Acoust. Soc. Am.*, **130**(4), 2512, (2011).

23. S.A. McInerny, G. Lu and S. Olcmen, "Rocket and Jet Mixing Noise, Background and Prediction Procedures", Under Contract UM 03-08-013, National Center for Physical Acoustics, University of Mississippi, (2004).

24. J. Laufer, R. Schlinker and R.E. Kaplan, "Experiments on Supersonic Jet Noise", *AIAA J.*, **14**(4), 489–497, (1976).

25. C.K.W. Tam, K. Viswanathan, K.K. Ahuja and J. Panda, "The sources of jet noise: Experimental evidence", *J. Fluid Mech.*, **615**, 253–292, (2008).

26. C.K.W. Tam, M. Golebiowsky and J.M. Seiner, "On the Two Components of Turbulent Mixing Noise from Supersonic Jets", AIAA Paper 96-1716, (1996).

27. T.B. Neilsen, K.L. Gee, A.T. Wall and M.M. James, "Comparison of near-field military jet aircraft noise with similarity spectra", *J. Acoust. Soc. Am.*, **129**(4), 2442, (2011).

28. K.L. Gee, T.B. Gabrielson, A.A. Atchley and V.W. Sparrow, "Preliminary Analysis of Nonlinearity in Military Jet Aircraft Noise Propagation", *AIAA J.*, **43**(6), 1398–1401, (2005).

29. D.K. McLaughlin, C.-W. Kuo and D. Papamoschou, "Experiments on the Effect of Ground Reflections on Supersonic Jet Noise", AIAA Paper 2008-22, (2008).

30. T.D. Norum, D.P. Garber, R.A. Golub, O.L. Santa Maria and J. S. Orme, "Supersonic Jet Exhaust Noise at High Subsonic Flight Speed", NASA/TP-2004-212686, (2004).

31. S. McInerny, K.L. Gee, M. Dowing and M. James, "Acoustical nonlinearities in aircraft flyover data", AIAA Paper 2007-3654, (2007).

32. J. Morgan, "Simple-source model of military jet aircraft noise", Senior Thesis, Department of Physics and Astronomy, Brigham Young University, (2011).

33. J. Morgan, K.L. Gee, T.B. Neilsen and A.T. Wall, "A simple-source model of military jet aircraft noise radiation", *Noise Control Engr. J.*, **60**(4), 435–449, (2012).

34. T.B. Gabrielson, T.M. Marston, and A.A. Atchley, "Nonlinear propagation modeling: Guidelines for supporting measurements", *NoiseCon05*, (2005).

35. S.A. McInerny, "Launch Vehicle Acosutics Part 2: Statistics of the Time Domain Data", *J. Aircraft*, **33**(3), (1996).